1 Numerical Accuracy

Theoretically, if the same **DCF!** is used, all the algorithms mentioned in section **??** should give exactly the same energy $\mathcal{F}_{\text{exc}}$ and gradient γ, in the perfect condition that all the quantities are continuous (with infinite points of grid), the basis sets of **FFT!** and **FGSHT!** are complete (infinite number of $\mathbf{k}$ or order of expansion $n_{\max}$), and the system is border-free (infinite length of box). However, this is obviously impossible, and the errors due to such effects can be far from imperceptible within the level of discretization allowed by the computing capacity nowadays. This section works on all the possible effects and parameters that have an influence to the accuracy, e.g. the usage of different algorithms, or different discretizing parameters. The goal of this study is to determine in which conditions the errors can be regarded as negligible; it thus gives a global view of the credibility for the results given by this code.

1.1 Generalized spherical harmonics transform

As discussed in §**??**, a discretized function $F(\Theta,\Phi,\Psi)$ after a forward-backward **GSHT!** process (eq. (**??**-**??**))

$$F^m_{\mu'\mu}=\frac{f_m}{8\pi^2}\sum_{i=0}^{m_{\max}} w_i \sum_{j=0}^{2m_{\max}} \sum_{k=0}^{2\lfloor m_{\max}/s\rfloor} F(\Theta_i,\Phi_j,\Psi_k)R^{m*}_{\mu'\mu}(\Theta_i,\Phi_j,\Psi_k) \tag{1.1}$$

$$F(\Theta_i,\Phi_j,\Psi_k)=\sum_{m=0}^{n_{\max}} f_m \sum_{\mu'=-m}^{m} \sum_{\substack{\mu=-m\\ \text{mod }(\mu,s)=0}}^{m} F^m_{\mu'\mu}R^m_{\mu'\mu}(\Theta_i,\Phi_j,\Psi_k) \tag{1.2}$$

only remains the same when:

1. F can be expanded on **GSH!**s of order at most $n_{\max}$ in eq. (1.2), thus it is always the case that F is a polynomial of both $\cos\Theta$, $\cos\Phi$ and $\cos\Psi$ of order n, where $n\leq n_{\max}$;
2. The order of quadrature $m_{\max}$ used in the **GSH!** expansion in eq. (1.1) should be larger than the order of the polynomial F, which means $n\leq m_{\max}$;

The two rules are quite evident. It should be also noted that as we do first a forward then a backward transform, when $m_{\max}<n_{\max}$, even the input function is of order at most $m_{\max}$; the output function is of order $n_{\max}$ in the presence of $R^m_{\mu'\mu}$ which is of order $n_{\max}$. That means F is no longer the same. Therefore, the forward-backward error is also controlled by the relation between the two discretizing parameters:

3. $m_{\max}\geq n_{\max}$ is needed to ensure the absence of accuracy loss.

In reality, the density variable $\rho(\mathbf{r},\mathbf{\Omega})$ and the gradient $\gamma(\mathbf{r},\mathbf{\Omega})$ that should be expanded via **FGSHT!** are never a simple polynomial. It is important to understand how much the choice of $m_{\max}$ and $n_{\max}$ will affect the accuracy, as they are tightly linked to the performance. Therefore we chose some simple functions below to see what happens when the function does not meet the three conditions. Note that the **FFT!** process leads to

strictly no accuracy loss (at machine precision, approximatively 10^{-13}), which means the **FGSHT!** process will have strictly the same result with the **GSHT!** process. Here we do not need to distinguish the two.

1.1.1 $m_{\max}$ *and* $n_{\max}$ *of projections*

The numerical error tests of a forward-backward **GSHT!** process with different order $n_{\max}$ of **GSH!** and $m_{\max}$ of quadrature are shown in table 1.1 for various polynomials, the absolute error

$$E_{\mathrm{a}}(\mathbf{\Omega}) = \left| f^{\mathrm{before}}(\mathbf{\Omega}) - f^{\mathrm{after}}(\mathbf{\Omega}) \right| \tag{1.3}$$

being defined as the norm of difference in function $f(\mathbf{\Omega})$ after a forward-backward **GSHT!** process. The maximum absolute error $E_a^{\max}$ is the maximum value in $E_{\mathrm{a}}(\mathbf{\Omega})$.

From table 1.1 we can see that for function $f(\mathbf{\Omega}) = 1 = R_{00}^0$, $m_{\max} \geq 0$, $n_{\max} \geq 0$ and $m_{\max} \geq n_{\max}$ give a null difference. Similarly, function $f(\mathbf{\Omega}) = \cos 3\Theta = 4\cos^3\Theta - 3\cos\Theta$ is a polynomial of $\cos\Theta$ of order 3, which can be expanded on R_{00}^3 and R_{00}^1 terms; it should satisfy $m_{\max} \geq n_{\max} \geq 3$. $f(\mathbf{\Omega}) = \cos 3\Phi$ is a polynomial of $\cos\Phi$ of order 3, but it cannot be expanded on **GSH!**s. In fact, all the functions in which the order of $\cos\Phi$ and $\cos\Psi$ is greater than $\cos\Theta$ cannot be expanded on a finite number of **GSH!**s. R_{30}^3 can expanded on itself, and indeed a polynomial of order 3 requiring $m_{\max} \geq n_{\max} \geq 3$.

We can see that, all the $E_a^{\max}$ where $m_{\max} < n_{\max}$ is are rather large, and fortunately we use only $m_{\max} \geq n_{\max}$ in **FGSHT!** for numerical reasons. Yet the $E_a^{\max}$ for $m_{\max} \geq n_{\max}$ may not be negligle either, knowing that the values of trigonometric functions are in between $[-1, 1]$. However, if the most portion of the function is a polynomial within the required order, the extra part does not play a great role, such that the total mean error is not as significant as seen now.

1.1.2 *From* ρ *to* γ

In the same way, the maximum absolute error of the density variable $\rho(\mathbf{r}, \mathbf{\Omega})$, which is not a combination of **GSH!**s, can be huge. It even gives the appearance of unphysical density $\rho(\mathbf{r}, \mathbf{\Omega}) < 0$ (i.e. $\Delta\rho(\mathbf{r}, \mathbf{\Omega})/\rho_0 < -1$) at certain points after a forward-backward **GSHT!** process, as shown in figure 1.1.

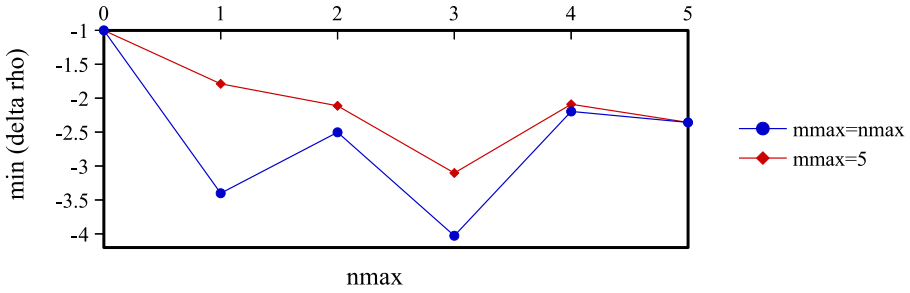

Figure 1.1: The minimum value of $\Delta\rho(\mathbf{r}, \mathbf{\Omega})/\rho_0$ after a forward-backward **GSHT!** process with respect to $n_{\max}$. Computed for a 45^3 grid ($L = 25$) for a converged density of an artificial charged LJ center $\mathrm{CH}_4^{+0.4}$.

Theoretically, we expect this minimum value to approach zero when increasing $m_{\max}$ or $n_{\max}$. This is not exactly the case. That means the order of expansion within the computing capacity ($n_{\max} \leq 5$) is still far from finding a tendency. If we look at the

rotational invariant expansion of $\rho(\mathbf{r},\mathbf{\Omega})$, which gives the projections $\rho^{0nl}_{0\nu}(r)$ (0 as the solute is spherical) shown in figure 1.2:

It is normal that the curves are a little noised because of the irregular grid histogram. Note that the projections $f^{mnl}_{\mu\nu}$ are purely real if f is real and μ, ν are even number.

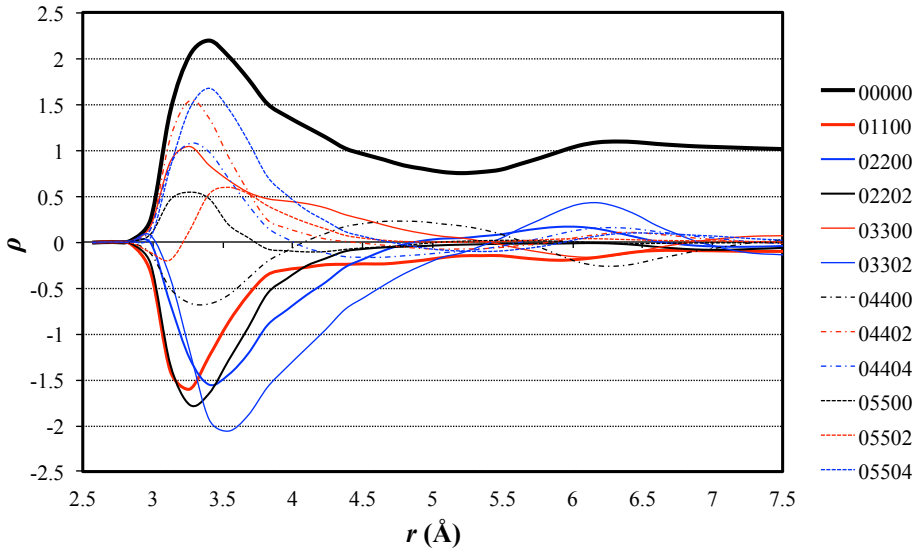

Figure 1.2: The projections $\rho^{0nl}_{0\nu}(r)$ computed for a 45^3 grid ($L = 25$) for a converged density of an artificial charged LJ center $CH_4^{+0.4}$

In figure 1.2, we observe that the first peaks of projections of higher order are still non-negligible. That gives the tendency in figure 1.1. The first projection $\rho^{000}_{00}(r)$ is purely positive, such that the minimum of ρ is zero; when the more negative projections are added on to the combined function, this error will go to negative. The minimum will have a tendency to converge only if the order of projections are above the current order 5.

That means within the computing capacity, we cannot correctly expand the density ρ on **GSH!**s. However, in the code MDFT, the density ρ is generated by minimization process determined by the gradient of energy γ. Note that $\hat{\gamma}(\mathbf{k},\mathbf{\Omega})$ is a convolution product, where $\Delta\hat{\rho}(\mathbf{k},\mathbf{\Omega})$ and the **DCF!** $\hat{c}(k,\mathbf{\Omega}_1,\mathbf{\Omega}_2)$ can be both expanded on **GSH!**s and rotational invariants. Therefore, the higher order terms vanish more easily in $\hat{\gamma}$, as they are the product of higher order terms of $\Delta\hat{\rho}(\mathbf{k},\mathbf{\Omega})$ and $\hat{c}(k,\mathbf{\Omega}_1,\mathbf{\Omega}_2)$. We see in figure 1.3 that the first terms of γ is much stronger than the terms of $n = 3, 4, 5$. Therefore we can consider that the expansion of γ already converge within $n_{\max} \leq 5$, even $n_{\max} \leq 3$.

1.2 COMPARISON BETWEEN BRANCHES

The algorithms mentioned in section **??** should give the same result if the same **DCF!** is used, in the condition that the error due to discretization is not fatal. The most direct comparison can be done with the free energy and structure obtained at the end of minimization. To be more strict, it is also worthwhile to study only the $\mathcal{F}_{\text{exc}}$ functional evaluation during one iteration without minimization, i.e. the process shown in figure **??**. In this scope, $\gamma(\mathbf{r},\mathbf{\Omega})$ becomes a better detailed criteria than $\mathcal{F}_{\text{exc}}$ to be compared.

1.2.1 *Difference in energy evaluation*

If we compare two results calculated analytically, the difference between them should be at machine precision if they are strictly equivalent. However, during the minimiza-

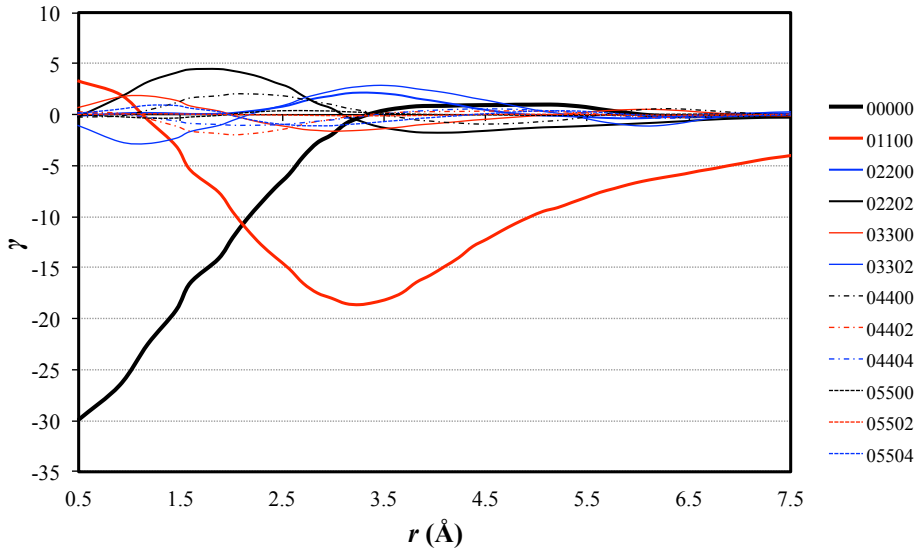

Figure 1.3: The projections $\gamma_{0\nu}^{0nl}(r)$ computed for a 45^3 grid ($L = 25$) for a converged density of an artificial charged LJ center $CH_4^{+0.4}$

tion process, the convergence of final free energy is normally controlled by imposed criteria. Two are used in code MDFT: $\varepsilon_{\mathcal{F}}$ is the difference between the free energies of the last two iterations, and $\|\text{projg}\|_\infty$ is the norm of the projected gradient in L-BFGS-B [**Zhu__1994__bfgs**, **Zhu__bfgs__1997__algorithm**]. The minimization is thought to converge if one of the criteria is met.

We use the implementation of the code to measure how much significant digits we can obtain with such criteria. As shown in table 1.2, in this thesis we use three types of criteria. In normal conditions, the free energy can converges to three decimal after point. In case of convergence difficulty, as for some molecular solutes, looser criteria can be used.

CRITERIA	WELL CONVERGED	CONVERGED (CHEM. ACCURACY)	LOOSE CONVERGENCE
$\varepsilon_{\mathcal{F}}$	< 0.00001	< 0.001	< 0.01
$\|\text{projg}\|_\infty$	< 0.00001	< 0.0001	< 0.001
$\mathcal{F}^{H_2O}$	$-70.601(-0.003)$	$-70.4(-0.2)$	$-68(-3)$
$\mathcal{F}^{CH_4^+}$			

Table 1.2: Minimized free energy $\mathcal{F}$ given by different convergence criteria. Test of solute water SPC/E, with dipole **DCF!**, $L = 24$ Å, nfft $= 72$; which gives a converged free energy (-70.60436 kJ $\cdot$ mol^{-1}) in very strict criteria.

Illustrated in table 1.3, the different methods listed in table **??** and using the same **DCF!** give nearly the same total free energy at the end of minimization.

METHOD	$n_{\max}$	DCF	FREE ENERGY (kJ/mol)
`dipole`	1	[**zhao_accurate_2013**]	13.965
`naive_dipole`	1	[**zhao_accurate_2013**]	13.965
`convolution_standard`	1	[**zhao_accurate_2013**]	13.965
`naive_standard`	1	[**puibasset_bridge_2012**]	19.224
`naive_interpolation`	1	[**puibasset_bridge_2012**]	19.434
`naive_nmax1`	1	[**puibasset_bridge_2012**]	19.225
`convolution_standard`	1	[**puibasset_bridge_2012**]	19.225
`convolution_asymm`	1	[**puibasset_bridge_2012**]	19.225
`convolution_pure_angular`	1	[**puibasset_bridge_2012**]	19.225
`naive_standard`	3	[**puibasset_bridge_2012**]	26.105
`naive_interpolation`	3	[**puibasset_bridge_2012**]	26.971
`convolution_standard`	3	[**puibasset_bridge_2012**]	26.105
`convolution_asymm`	3	[**puibasset_bridge_2012**]	26.105
`convolution_pure_angular`	3	[**puibasset_bridge_2012**]	26.105

Table 1.3: Minimized free energy via different branches MDFT of a charged $CH_4^{+0.33}$ LJ center calculated for a 33^3 ($L = 20$Å) grid. Gauss-Legendre quadrature is used as Θ angle grid, with $m_{\max} = n_{\max}$.

In table 1.3, we can see that apart from **`naive_interpolation`**, all branches give the same result if other parameters are fixed. The slight difference due to the interpolation error is also acceptable (in this case); and the error due to the **GSH!** expansion (difference between for instance **`naive_standard`** and **`convolution_standard`**) seems to be well compensated during the minimization. This also supports the conclusion above that in fact we just need a lower expansion of **GSH!** for γ than for $\Delta\rho$.

1.2.2 *A single k-kernel*

If we want to compare within one evaluation of $\mathcal{F}_{\text{exc}}$ as shown in figure **??**, we can be first interested in the local paths from $\Delta\hat{\rho}^m_{\mu'\mu}(\mathbf{k})$ to $\hat{\gamma}^m_{\mu'\mu}(\mathbf{k})$ that can be tested independently for a given $\mathbf{k}$. Referring to figure 1.4, four algorithms are available for such a purpose:

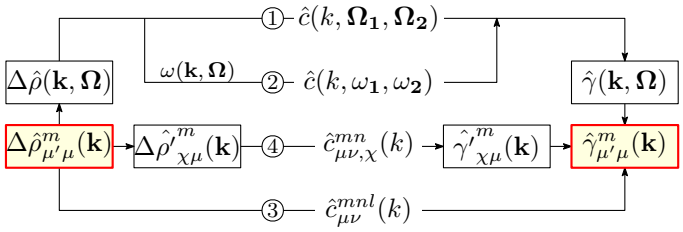

Figure 1.4: A k-kernel

A program to compare each element of $\hat{\gamma}^m_{\mu'\mu}(\mathbf{k})$ issued from these four algorithms for a given $\Delta\hat{\rho}^m_{\mu'\mu}(\mathbf{k})$ shows that the $\hat{\gamma}^m_{\mu'\mu}(\mathbf{k})$ for the four algorithms are strictly identical, i.e. the maximum error is at machine precision. This means the final result of energy and structure is independent to the choice of path inside a k-kernel, if $\Delta\hat{\rho}(\mathbf{k}, \mathbf{\Omega})$ can be fully expanded on **GSH!**s.

1.2.3 *k-border effect*

The next step is to test the whole process shown in figure **??**. Theoretically, if $\Delta\rho(\mathbf{r},\mathbf{\Omega})$ is generated from a recombination of **GSH!** projections $\Delta\rho^m_{\mu'\mu}(\mathbf{r})$, all the branches should give mathematically the same gradient $\gamma(\mathbf{r},\mathbf{\Omega})$.

The detailed error value of γ here has not been noted, as it was regarded as a bug in the code at that time, then the code has since been modified. But in fact, the choice to add corrections or not on the even number grid is not something about right and wrong.

Firstly, we compare the three **convolution** algorithms passing by **GSH!** expansion. For a 64^3 grid, $n_{\max}=3$, the three algorithms **convolution_standard**, **convolution_asymm**, and **convolution_pure_angular** give the same $\mathcal{F}_{\text{exc}}$ at first sight, but somewhat different results when comparing each element of $\gamma(\mathbf{r},\mathbf{\Omega})$. The perceived difference seems to decrease when increasing the number of grid points. Moreover, $\gamma(\mathbf{r},\mathbf{\Omega})$ recombined from projections $\gamma^m_{\mu'\mu}(\mathbf{r})$, which should be purely real as explained in §**??**, have a slight imaginary part. Surprisingly, for a 65^3 grid, it gives numerically the same $\gamma(\mathbf{r},\mathbf{\Omega})$ for all three algorithms at machine precision. The theory behind this behavior is found to be a special k-border effect linking to an even number of nodes in any dimension of the grid.

As the symmetry

$$\Delta\hat{\rho}'^m_{\chi\mu}(\mathbf{k}) = (-)^{m+\mu+\chi}\Delta\hat{\rho}'^{m*}_{\chi\underline{\mu}}(-\mathbf{k}) \tag{1.4}$$

is generated by two symmetries

$$\Delta\hat{\rho}^m_{\mu'\mu}(\mathbf{k}) = (-)^{\mu'+\mu}\Delta\hat{\rho}^{m*}_{\underline{\mu'}\mu}(-\mathbf{k}) \tag{1.5}$$

$$R^m_{\mu'\chi}(\hat{\mathbf{k}}) = (-)^{m+\mu'+\chi}R^m_{\underline{\mu'}\chi}(-\hat{\mathbf{k}}) \tag{1.6}$$

For the k points "at border", i.e. after the **FFT!** where the point having $\pm k_i = k_i^{\max}$, $i=1,2,3$, for example for k_1,

$$\Delta\hat{\rho}^m_{\mu'\mu}(\pm k_1,k_2,k_3) = \Delta\hat{\rho}^m_{\mu'\mu}(k_1^{\max},k_2,k_3) \tag{1.7}$$

is naturally put in the same array by FFT for the grids of an even number, as shown in figure 1.5.

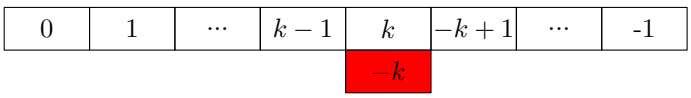

Figure 1.5: k-border effect

For example, for a grid 1D, the FFT having 6 points gives the values for indices 0,1,2,3,-2,-1, and the FFT having 7 points gives the values for 0,1,2,3,-3,-2,-1.

As **FFT!** possesses periodicity, the symmetry 1.10 can always be respected at the border. However, as

$$R^m_{\underline{\mu'}\chi}(-\hat{k}\equiv(-k_1,-k_2,-k_3)) \neq R^m_{\mu'\chi}(k_1^{\max},-k_2,-k_3) \tag{1.8}$$

the symmetries (1.6) and (1.4) are not respected for these points. In the backward process, if we account for all the $\gamma^m_{\mu'\mu}(\mathbf{k})$, as

$$\gamma^m_{\mu'\mu}(-\hat{k}\equiv(-k_1,-k_2,-k_3)) \neq \gamma^m_{\mu'\mu}(k_1^{\max},-k_2,-k_3) \tag{1.9}$$

the symmetry

$$\gamma^m_{\mu'\mu}(\mathbf{k}) = (-)^{\mu'+\mu}\gamma^{m*}_{\underline{\mu'}\mu}(-\mathbf{k}) \tag{1.10}$$

is not totally respected, and this imposes that $\gamma^m_{\mu'\mu}(\mathbf{r})$ has a imaginary part. This imaginary part has been omitted implicitly in the "real to complex" **FFT!** process used in, for example, **FGSHT!** in **convolution_standard**, or **FFT!**3D in **convolution_pure_angular**. That is to say, we keep only the part of nonnegative $\mathbf{k}$ or nonnegative μ, supposing that the part we omit respects the symmetry.

In the purpose that the three algorithm gives the same result, we can artificially impose at the border:

$$R^m_{\mu'\chi}(k_i^{\max}) = \frac{1}{2}\left[R^m_{\mu'\chi}(k_i) + R^m_{\mu'\chi}(-k_i)\right] \tag{1.11}$$

where i is the conflict index in figure 1.5. If more than one dimension is in conflict, this process can be done twice (4 terms for "edges" of the cube) or three times (8 terms for "vertices"). The point $\mathbf{k} = \hat{0}$ is different; as it is defined along the z-axes to avoid underdetermination, it does not respect eq. (1.6) and (1.4), neither. However, this point is proven to be negligible compared to the hundreds of thousands of total points.

1.2.4 *Difference in γ for "naive" and "convolution" methods*

In the same way, we compare the $\mathcal{F}_{\text{exc}}$ and $\gamma(\mathbf{r}, \mathbf{\Omega})$ given by branches **`naive_standard`** and **`convolution_standard`**. The $\mathcal{F}_{\text{exc}}$ of these two branches are identical for a 65^3 and $n_{\max} = 3$ grid, but the elements of $\gamma(\mathbf{r}, \mathbf{\Omega})$ have a difference at order of 10^{-2} to 10^{-3} which seems to be random. A test redone for a 45^3 grid is shown in figure 1.6.

According to figure 1.6, we can hypothesize that this error depends on the angular quadrature $m_{\max}$. The dependence is natural, as the difference between algorithms **`naive`** and **`convolution`** is the treatment of the angular part. There is also a dependence on L in the k-space, but after **FFT!** it is mixed. The increase of error in the $n_{\max}$ chart is unnatural, implying there is still something theoretical that we have missed, or a bug in the code.

In short, this troublesome difference cannot be yet explained, as the **`naive`** methods do not have a k-border effect linked to symmetry, and in fact we used an odd grid. The projections $\gamma^{mnl}_{\mu\nu}(r)$ of these two algorithms seem to be identical (figure 1.7), which is to say that the global profile of the two should be almost the same, and thus the error would not be very decisive. Knowing that the difference is even more compensated with many iterations as shown in table 1.3, we can consider that this slight difference has no consequence to the final result.

1.3 INTRINSIC VARIATION OF FREE ENERGY

The comparison between branches shows that there is no significant difference between the branches, if other parameters are all fixed. Therefore one is free to study the dependence on discretizing parameters with one or another algorithm.

Before studying the dependence on expansion order $m_{\max}$ and $n_{\max}$, we are interested in the spatial grid dependance, as well as the Ψ grid dependance if it is not automatically fixed by $m_{\max}$ (figure 1.8), which can have an influence on the tests later.

Looking at figure 1.8 (a) and (b), we show that the resolution of the spatial grid has an effect on the calculated free energy. For the charged solute $CH_4^{+0.33}$, the energy has a tendency to decrease when increasing the resolution of grid (nfft). This decrease does not link to the border correction mentioned in §**??**, as both the box length and the charge remain the same for the whole set of test. From (b) we consider that at least a 3 points grid in 1 dimension (each direction) per Angstrom is needed to reduce the uncertainty due to grid resolution. Figure (c) is also neutral, i.e. does not need any border correction neither. We see that the energy also varies with respect to the box length (with direct summation this time), and have the same tendency for different resolution nfft/L. The curves of $\text{nfft}/L = 3$ and $\text{nfft}/L = 4$ do not give too much difference. Figure (d) fixed the Lebedev quadrature for Θ and Φ, but left varying the Ψ. We can also see a dependence on Ψ. which does not completely have a tendency to vanish when increasing the resolution

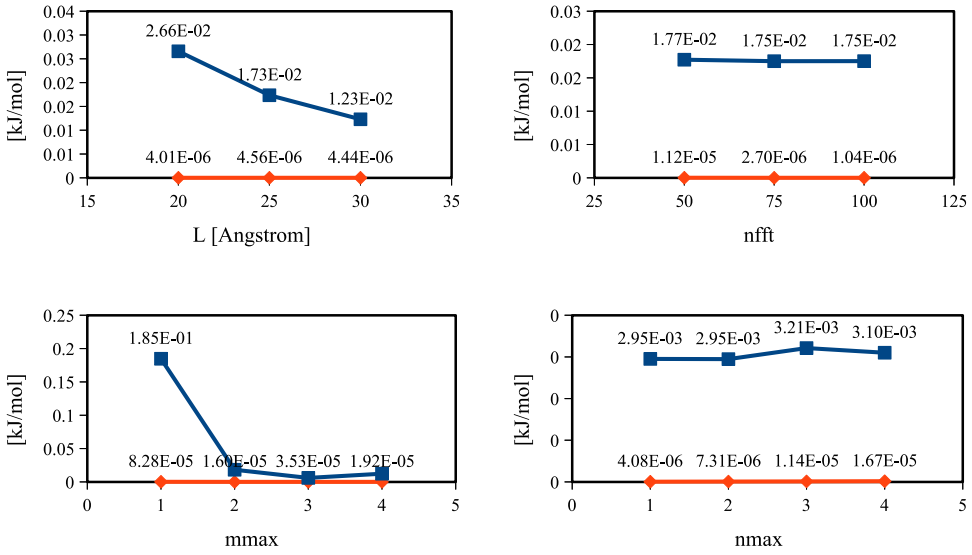

(a) $\delta\left[k_{\mathrm{B}}T\rho_0\hat{\gamma}(\mathbf{k},\mathbf{\Omega})\right]$

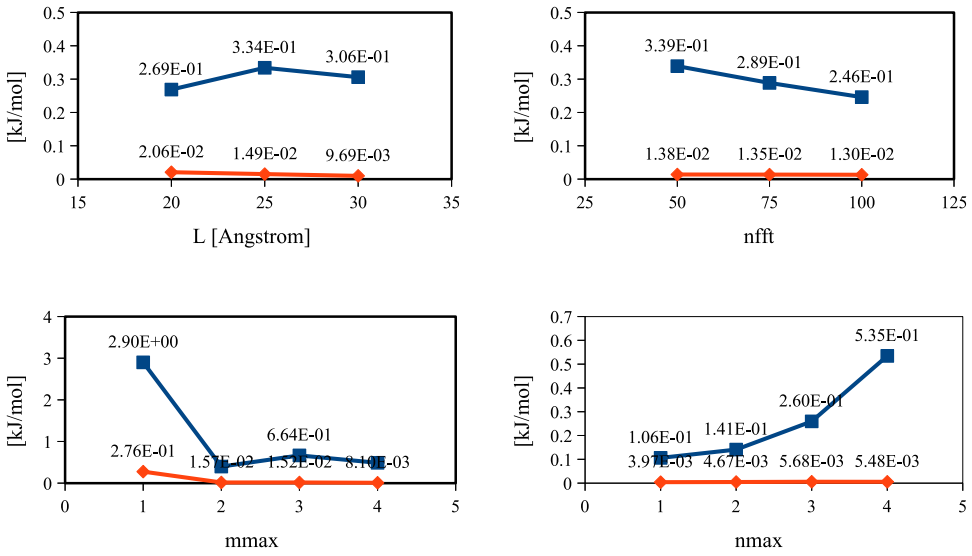

(b) $\delta\left[k_{\mathrm{B}}T\rho_0\gamma(\mathbf{r},\mathbf{\Omega})\right]$

Figure 1.6: Maximum (blue) and average (red) absolute difference in $\hat{\gamma}(\mathbf{k},\mathbf{\Omega})$ and $\gamma(\mathbf{r},\mathbf{\Omega})$ (normalized with $k_{\mathrm{B}}T\rho_0$), for tests of: (1) different box length L, with nfft = 65, $m_{\max} = n_{\max} = 2$; (2) different number of grid nfft^3, with $L = 25$ Å, $m_{\max} = n_{\max} = 2$; (3) $n_{\max} = 1$ to 4 for $m_{\max} = n_{\max}$ with 45^3 grid ($L = 25$ Å); (4) $n_{\max} = 1$ to 4 for $m_{\max} = 5$ with 45^3 grid ($L = 25$ Å). The test of $m_{\max} = n_{\max} = 5$ with 45^3 grid ($L = 25$ Å) is dropped as it takes too long. All the tests uses a converged density $\rho(\mathbf{r},\mathbf{\Omega})$ of an artificial charged LJ center $CH_4^{+0.4}$, recombined from **GSH!** projections of corresponding order $m_{\max}$ and $n_{\max}$.

of grid. Since during the whole thesis the Ψ is theoretically fixed in the same order (as) with Θ and Φ, this remains an issue for further verification. We can roughly conclude that an error around 1-2 kJ/mol is common for this code. The spatial grid dependence will not be treated in this thesis as it comes from other terms of the functional.

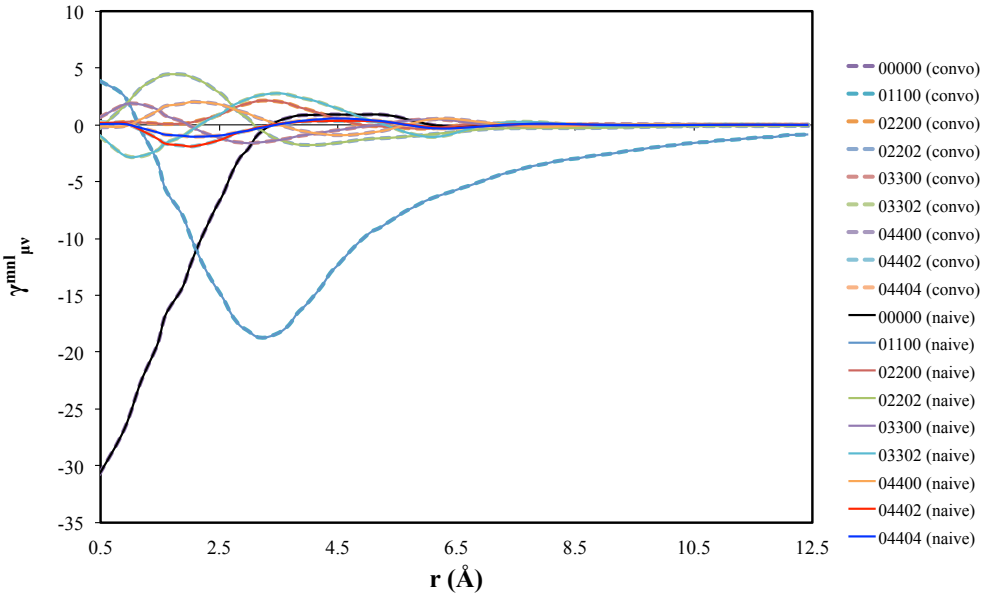

Figure 1.7: Comparison of projections $\gamma_{0\nu}^{0nl}(r)$ for branches "naive_standard" and "convolution_standard", computed with a 45^3 grid ($L = 25$) for a converged density of an artificial charged LJ center $CH_4^{+0.4}$.

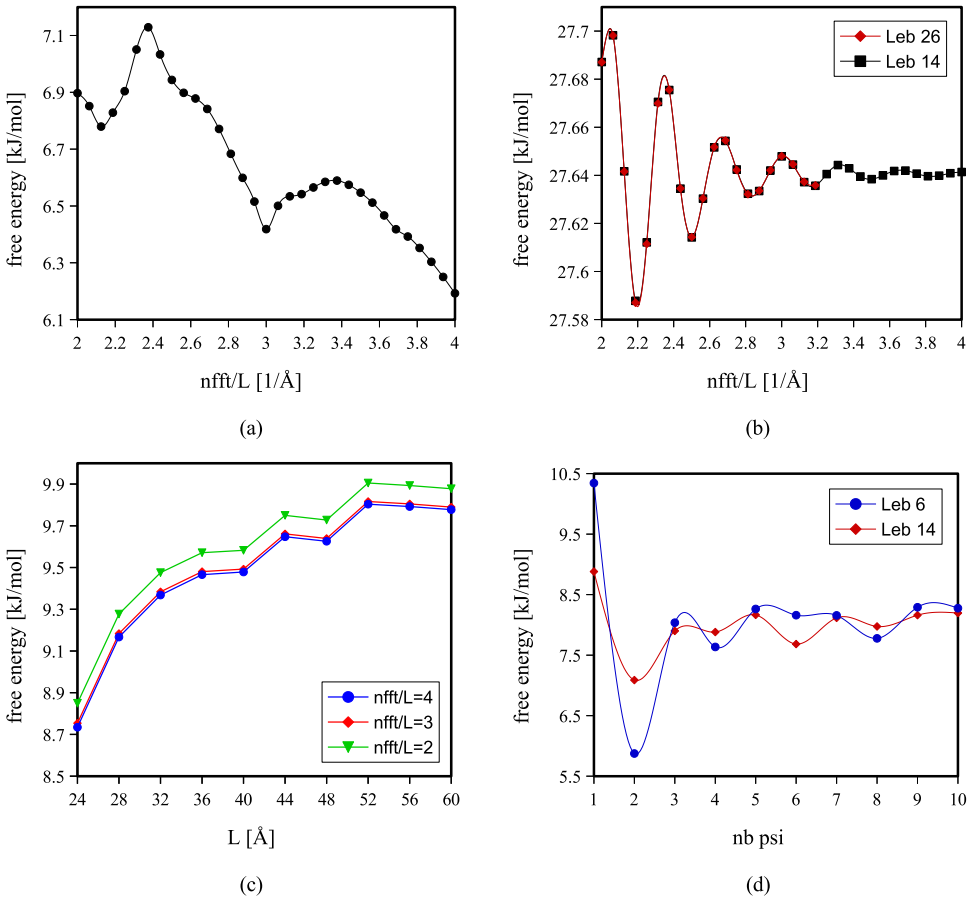

Figure 1.8: Space-grid and Ψ dependence of code **MDFT!**. (a) $CH_4^{+0.33}$ using dipole **DCF!** with $n_{\max} = 1$, $L = 32$ Å; (b) CH_4 using **DCF!** of $n_{\max} = 5$, $L = 32$ Å, Lebedev quadrature of order 2 or 3; (c) acetone using dipole **DCF!**, Lebedev quadrature 1 and 1Ψ angles, $\text{nfft}/L = 2, 3, 4$, using direct summation; (d) acetone using dipole **DCF!** and Lebedev quadrature 1 or 2, varying Ψ, $L = 32$ Å, nfft = 96.

1.4 SERIES OF CHARGED LJ CENTERS

To validate the method by comparing with **IET!**, as well as to study the dependance on $m_{\max}$ and $n_{\max}$, we firstly chose a series of LJ centers, which possess the LJ parameters of CH_4 [**asthagiri_role_2008**], and have a variable charge from -1.0 to 1.0 (table 1.4).

*For both IET and DM results in this thesis, 298K is used according to habitude instead of 303K recommended in reference [**SPC/E**]. For MDFT, 300K and 298K are used.*

1.4.1 *Box length dependance and charge dependance of free energy*

As discussed in section **??**, for single ions, two types of corrections need to be added on the free energy, which depend on the box length and charge of the ion. To verify these dependencies, we implement a systematic calculation with variable charge and box length using 3 different methods, the parameters of which are shown in table 1.5. It should be noted that, the **`naive_interpolation`** only used 14 Lebedev and 3 Ψ angles to converge, which gives exactly the same result with 26 Lebedev and 4 Ψ angles. That means the **`naive`** methods do not need an order of quadrature $m_{\max}$ to be greater than the order of **DCF!** $n_{\max}$.

*Some points of negative charge diverged; (in **IET!**, the negative charge also have difficulty to converge), and all the converged results are presented.*

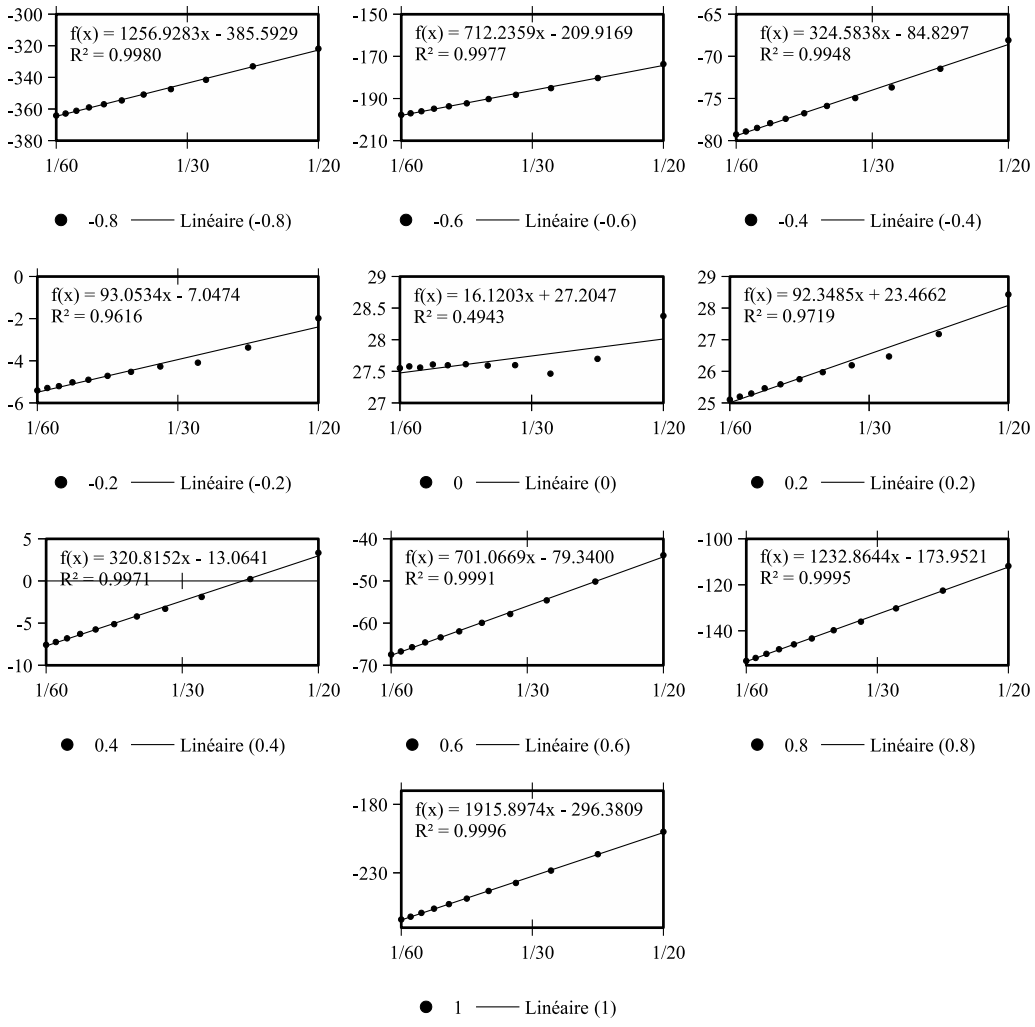

Figure 1.9: Free energy (without correction) of charged CH_4 center (-1.0 to 1.0) with respect to the box length, for **`naive_nmax1`** method, with 6 angles of Lebedev quadrature angles for Θ and Φ, 3 for Ψ, DCF of $n_{\max} = 1$, at 300K.

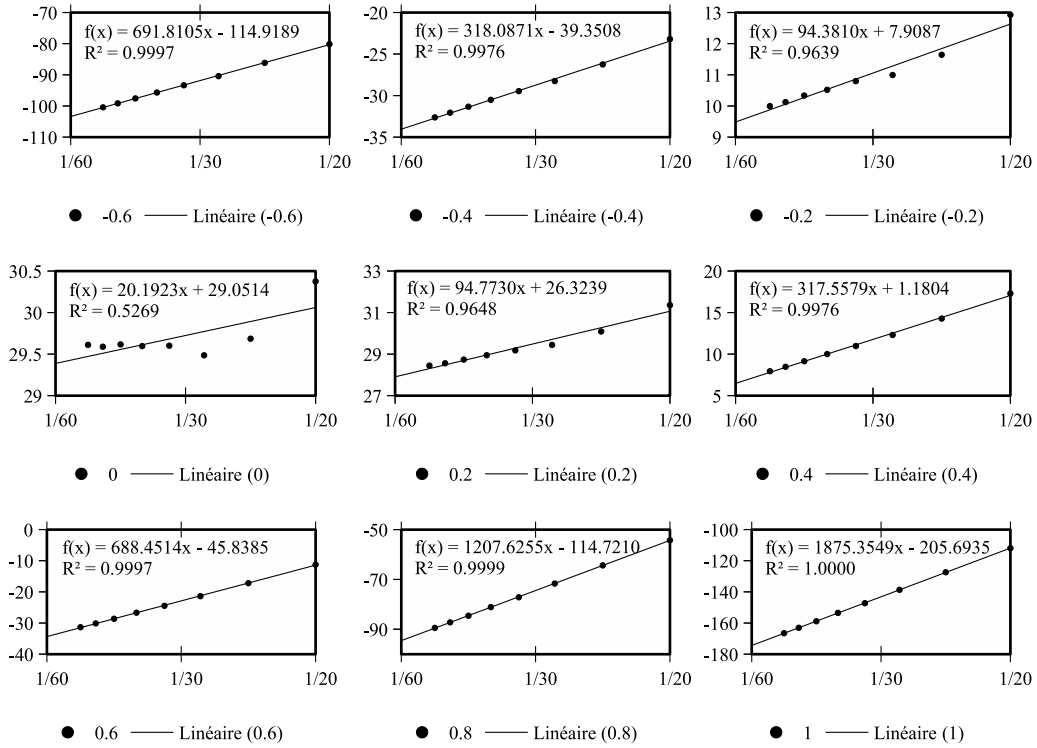

Figure 1.10: Free energy (without correction) of charged CH_4 center (-1.0 to 1.0) with respect to the box length, for **`naive_interpolation`** method, with 14 angles of Lebedev quadrature angles for Θ and Φ, 3 for Ψ, DCF of $n_{\max} = 5$, at 300K.

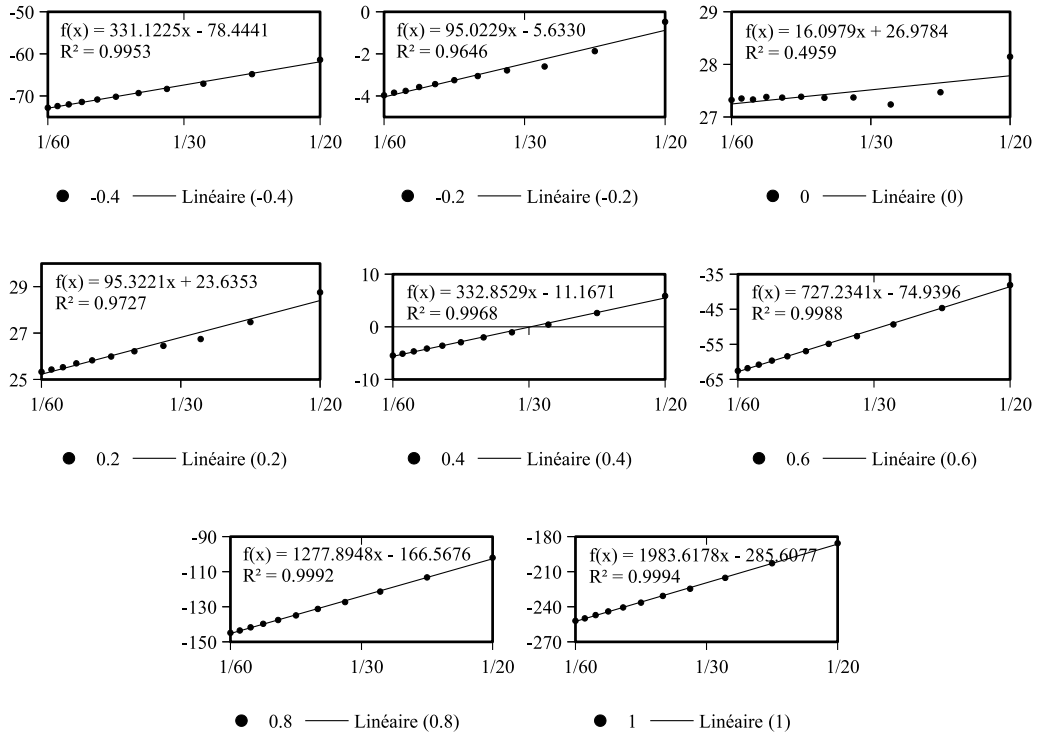

Figure 1.11: Free energy (without correction) of charged CH_4 center (-1.0 to 1.0) with respect to the box length, for **`convolution_standard`** method, with $m_{\max} = n_{\max} = 1$, at 298.15K.

The collections of the raw results issued directly from the code MDFT are shown in figure 1.9, 1.10 and 1.11. We can see that the dependence of box length for each charge is almost linear, except for the charge between $[-0.2, 0.2]$ (where grid dependence dominated compared to other effects). This means the influence of box length is much greater than the intrinsic variation of result mentioned in 1.3. The charge dependency of the slopes in these figures is traced in figure 1.12 with respect to $\mathfrak{q}^2$, square of the corresponding number charge. A linear regression is done to give the slope in figure 1.12 at 1937.8 $\mathrm{kJ \cdot mol^{-1} \cdot Å}$. This slope corresponds to the correction of type-B:

$$\frac{f_Q \xi}{2}\left(1 - \frac{1}{\varepsilon}\right) = 1943.2\,\mathrm{kJ \cdot mol^{-1} \cdot Å} \tag{1.12}$$

where $f_Q = q_e^2 10^{-3} N_\mathrm{A}/(4\pi\varepsilon_0 10^{-10})$ is the electrostatic potential unit so that $f_Q \cdot \mathfrak{q}^2/r$ is in $[\mathrm{kJ \cdot mol^{-1}}]$.

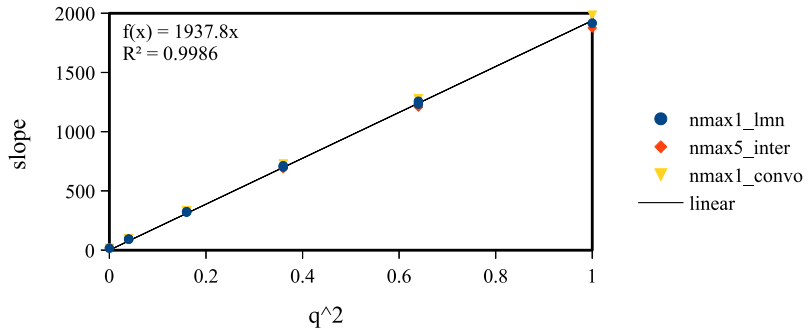

Figure 1.12: Quadratic charge dependence of free energy in $\mathrm{CH_4^{\mathfrak{q}}}$ series

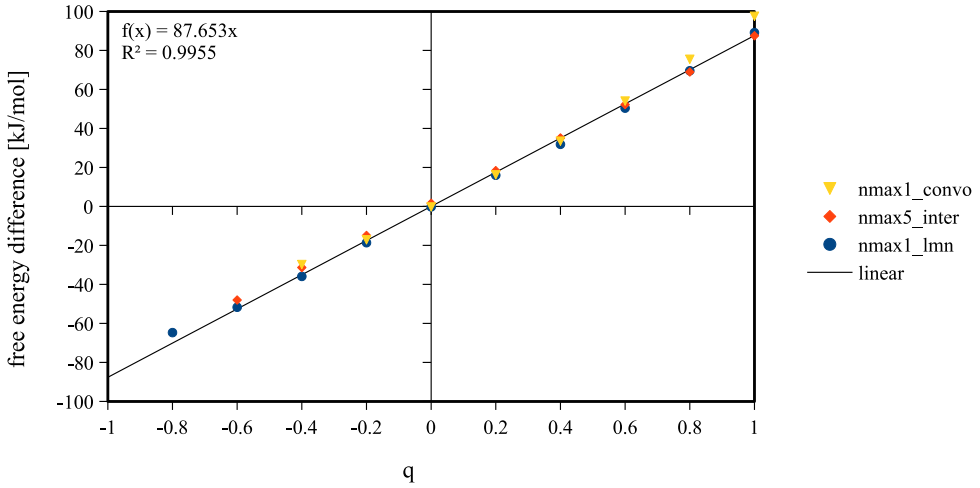

Figure 1.13: Free energy (extrapolated to infinite box length) of charged $\mathrm{CH_4}$ compared to **IET!**, without P-scheme correction

The intercept values in each of figures 1.9 to 1.11 correspond to the free energy of an infinite box. The **IET!** results to be compared are done with $R_\mathrm{max} = 102.4$Å, and need a correction of $-2.556 k_\mathrm{B} T$ to obtain the free energy in the infinite system. ("oui! préciser qu'il s'agit de calculs HNC "1D" 1 distance + 5 angles.": je ne comprends pas...) The difference in free energy between **MDFT!** and **IET!** of the infinite system are given in figure 1.13. The linear regression is done with all existing points in this figure, and its slope 87.653 $\mathrm{kJ \cdot mol^{-1}}$ corresponds to the correction of type-C:

$$\frac{2\pi}{3} f_Q \eta\gamma = 82.104\mathrm{kJ \cdot mol^{-1}} \tag{1.13}$$

The measured number and the theoretical one are a little different, it can be principally due to the lack of point at the -1 charge side.

1.4.2 *Comparison with IET after corrections*

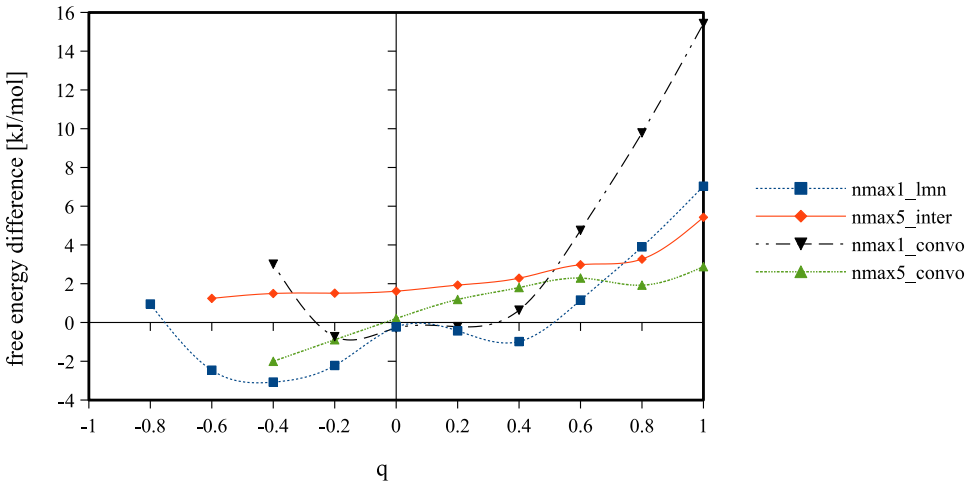

Figure 1.14: Free energy difference of CH_4^q series compared to IET, with all corrections

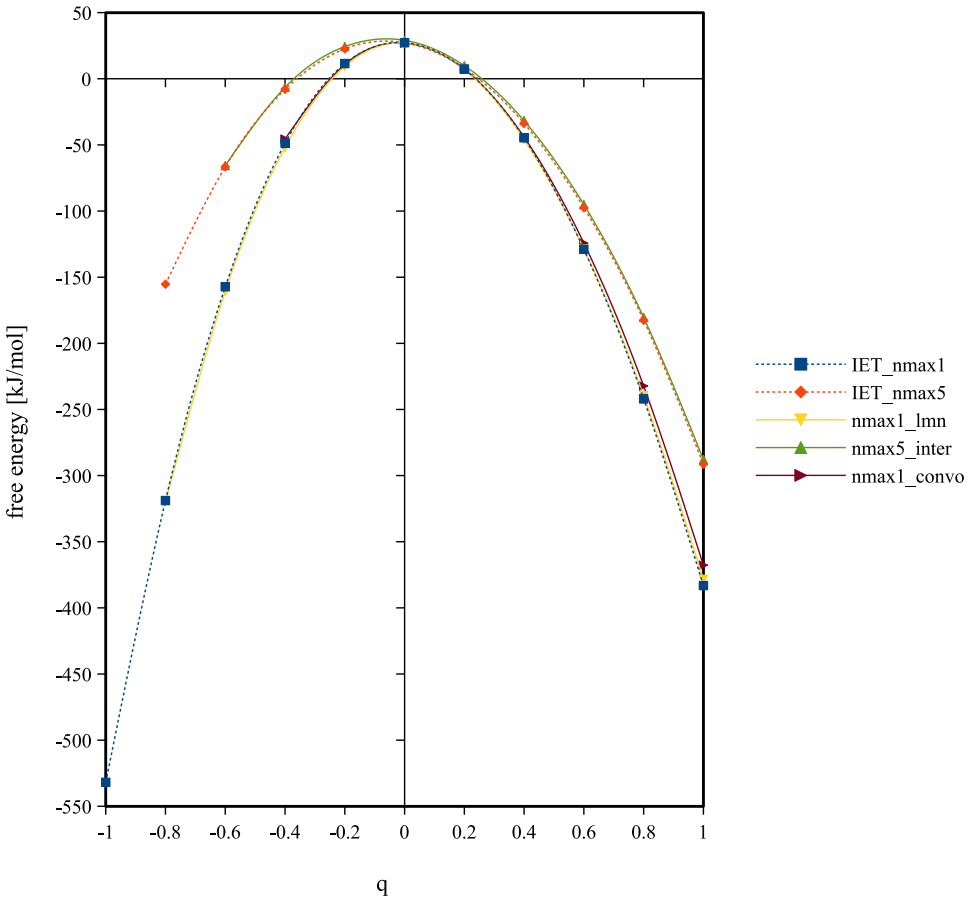

Figure 1.15: Free energy of CH_4^q series, with all corrections

The points in figure 1.13 after correction with eq. (1.13), as well as the difference between results of $m_{\max} = n_{\max} = 5$ given by `convolution_standard` (with $L = 24$ Å,

nfft = 72) using theoretical corrections and **IET!** with infinite corrections (nmax5_convo) are shown in figure 1.14. Note that the curves for the same **DCF!** are not perfectly in agreement with each other, unlike shown in table 1.3. The fact is that in "nmax1_lmn", Lebedev quadrature is used, and in "nmax1_convo", Gauss-Legendre quadrature is used, as we know the different angular grid can have an effect on the energy; and for $n_{\max} = 5$, as we have taken by chance the +0.4 as charge in table 1.3, the difference between the **`naive_interpolation`** and **`convolution_standard`** results are accidentally small. The troublesome energy shift of about 2 $\mathrm{kJ \cdot mol^{-1}}$ between "nmax5_inter" and **IET!** result is yet to understand, as well as the dependence on q for "nmax5_convo" after correction. But if we look at the free energies without comparing them in figure 1.15, we can see that these differences are almost negligible compared to the total energy they possess, and the curves only differs with different **DCF!**s.

1.4.3 *Dependence on $m_{\max}$ and $n_{\max}$*

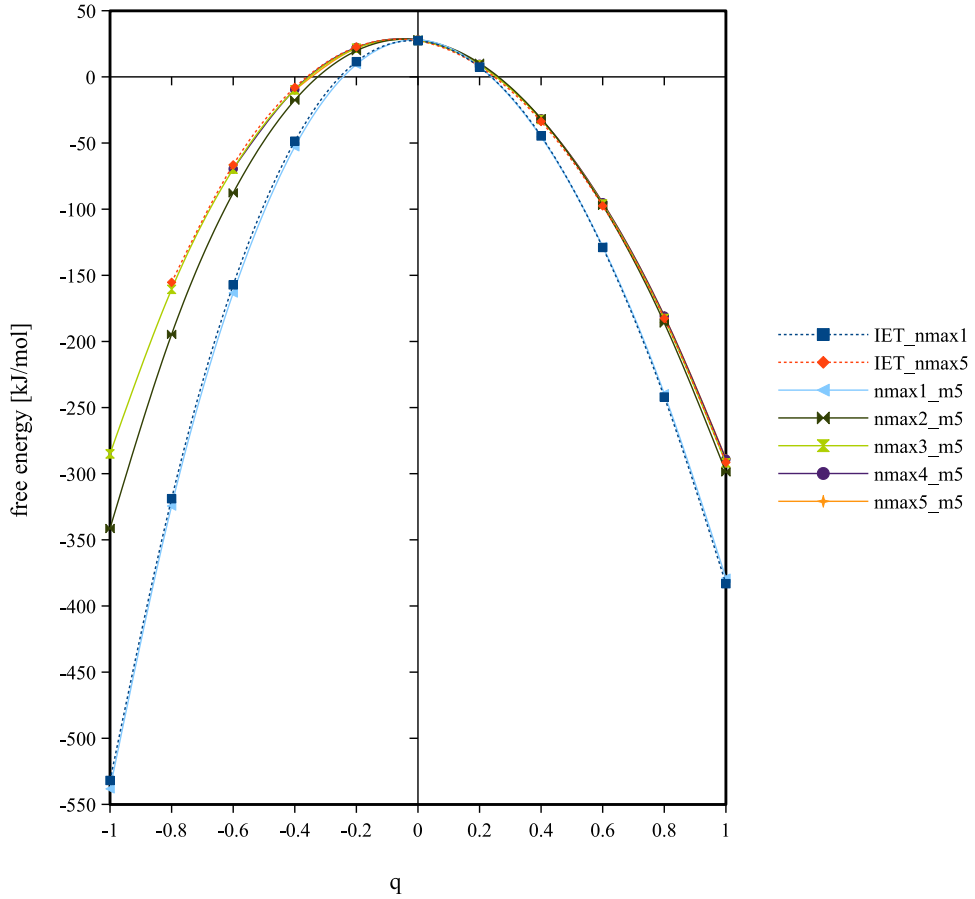

Figure 1.16: Free energy of CH_4^q series, with all corrections of **IET!** results and **MDFT!** $m_{\max} = 5$, $n_{\max} = 0, \ldots, 5$.

As we see, the free energy of charged CH_4^q series depends a lot on the order of **DCF!**, $n_{\max}$. To study systematically the influence of $m_{\max}$ and $n_{\max}$, we chose a series of tests with three charge: -0.6, 0, and +1, using **`convolution_standard`**, as shown in table 1.6. Three types of energy are listed: the results issued from **IET!**, the case when $m_{\max} = n_{\max}$ and $m_{\max} = 5$. As we said previously the gradient γ is smoother than ρ; it is worthwhile to study the case when the order of quadrature $m_{\max}$ for the expansion of ρ is larger than

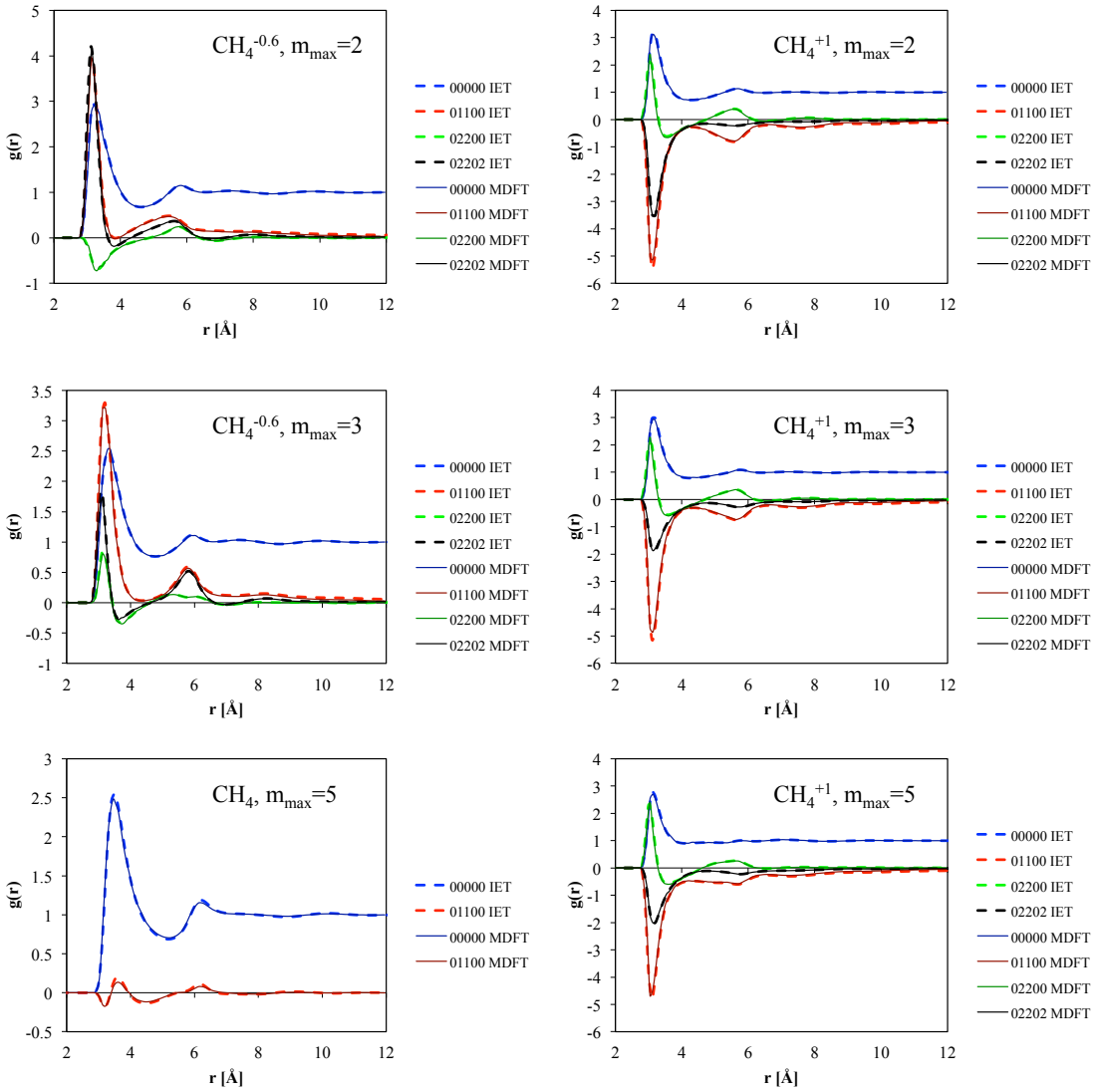

Figure 1.17: The projections $\rho_{0\nu}^{0nl}(r)$ of some selected charges of CH_4^q series comparing to **IET!**, with $m_{\max} = n_{\max}$.

the order of **DCF!** $n_{\max}$ used in equation **OZ!** to solve γ, in order to economize computing cost.

From table 1.6 we can see that the free energy becomes stable in any case when $n_{\max} \geq 3$; the free energies are quite in agreement with **IET!** results; and there is almost no difference between $m_{\max} = n_{\max}$ and $m_{\max} = 5$. That means, the quadrature of ρ have no influence to the final energy, which is yet comprehensible, as the extra order of quadrature gives no influence to the functional gradient, and the ρ used to evaluate the functional is given by minimization, i.e. without expansion on **GSH!**s.

A schema of free energy evaluation with respect to $n_{\max}$ ($m_{\max} = 5$, as some of the points of $m_{\max} = n_{\max}$ have difficulty to converge and if converge they give usually the same result) is made in figure 1.16. We see that from $n_{\max} = 3$ to higher order, the curves do not vary a lot. We can conclude that within $n_{\max} \geq 3$ to $n_{\max} = 5$, the error in free energy is acceptable.

Some selected projections $\rho_{0\nu}^{0nl}(r)$ (0 as solute is spherical) are compared to **IET!** in figure 1.17. We can see that they are in good agreement.

If we compare one charge in one graph, with all the $n_{\max}$, we can determine which $n_{\max}$ is sufficient to have a good structure of the density ρ. Figure 1.18 gives the zoomed

*We take solute-solvent formalism for **MDFT!**, and **IET!** takes the solvent-solute formalism. Thus in **MDFT!** the $g_{\mu\nu}^{mnl}$ corresponds to the $g_{\nu\mu}^{nml}$ in **IET!**. In figure*

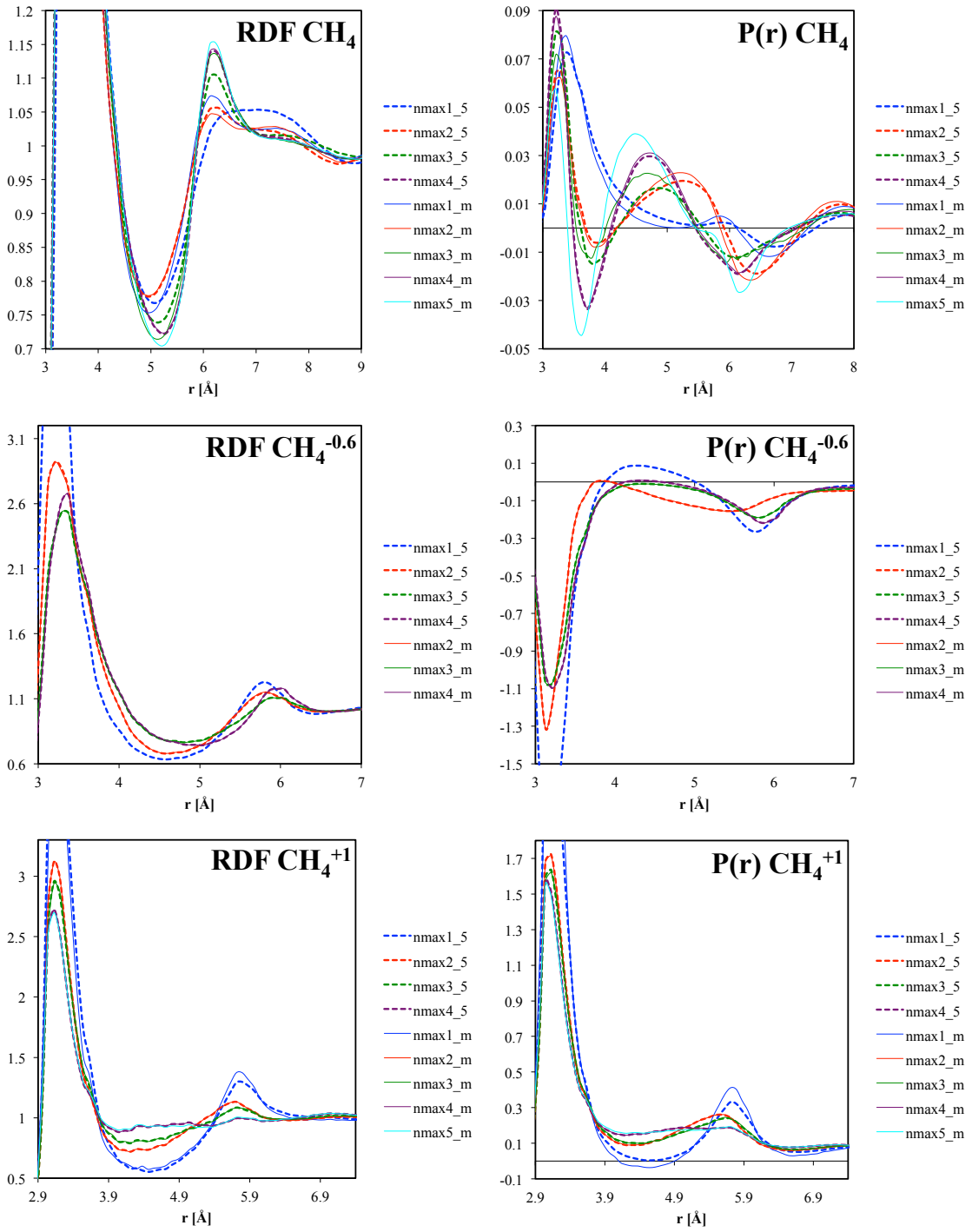

Figure 1.18: RDF and polarization of some selected charges of CH_4^q series with different $m_{\max}$ and $n_{\max}$

parts of **RDF!**s and **RDF!**s for the three charges, in order to have a clear view of only the different parts. Firstly we can see that in the most of cases, apart form uncharged CH_4 and some $n_{\max} = 1$, the curves of $m_{\max} = 5$ and $m_{\max} = n_{\max}$ are superposed. That means even for structure of single ions, extra order of $m_{\max}$ is useless. For -0.6, the curves converge from $n_{\max} = 3$, and for +1, $n_{\max} = 4$. For CH_4 it seems to be bazar, but looking at the scale of the schema and we consider that it converges from $n_{\max} = 4$. To conclude, for CH_4^q series, we think $n_{\max} = 3$ is sufficient for energy, and $n_{\max} = 4$ is

sufficient for structure to converge for common usages (without regarding to higher order projections).

1.5 UNCHARGED LJ CENTERS

As there is an energy shift between **`naive_interpolation`** and **IET!** results even for uncharged CH_4, we calculate some other uncharged LJ centers. Results in table 1.7 shows that this energy shift is common in any uncharged LJ centers.

SOLUTE	σ	ϵ	dipole	1	2	3	4	5	inter	**IET!**
Neon	3.035	0.15432	18.608	18.793	19.028	18.556	18.990	18.862	20.041	18.823
Argon	3.415	1.03931	22.155	22.465	22.858	22.146	22.722	22.389	24.238	22.270
Krypton	3.675	1.4051	25.356	25.763	26.228	25.483	26.137	25.733	27.823	25.493
Xenon	3.975	1.7851	29.678	30.241	30.766	30.125	30.735	30.249	32.658	29.918

Table 1.7: Free energy $[\mathrm{kJ \cdot mol^{-1}}]$ of rare gases, σ in [Å], ϵ in $[\mathrm{kJ \cdot mol^{-1}}]$, with $L = 24$ Å, nfft $= 72$.

1.6 LINEAR SOLUTES

To complete the story of $m_{\max}$ and $n_{\max}$ convergence, we choose some linear solutes shown in figure 1.19 and table 1.8. The direct summation method for $\mathcal{F}_{\mathrm{ext}}$ evaluation is used, as O_2 always diverge with Poisson method. We can make hypothesis that this is because the distance between the charges is to short, as shown in figure 1.19; therefore the interpolation in $\mathcal{F}_{\mathrm{ext}}$ evaluation can cause divergence. There is a better version of Poisson solver developing in parallel of this code, which has been reported of better convergence. We consider that this divergency problem does not come from the evaluation of $\mathcal{F}_{\mathrm{exc}}$.

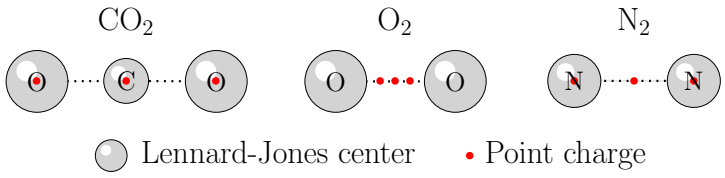

Figure 1.19: Test linear solutes

Table 1.9 shows the free energy of solute with respect to $n_{\max}$. We also find that from $n_{\max} = 3$, free energy seems to converge, and there is almost no difference between $m_{\max} = 5$ and $m_{\max} = n_{\max}$.

The structures of solutes are also compared to **IET!** results, shown in figure

Figure 1.20

1.7 PREMIER CONCLUSION

From the results, we see that **MDFT!** is capable to produce the same result with **IET!** for LJ centers, single ions and linear solutes. In a general feeling, **MDFT!** has an advantage

to calculate 3D molecules such as DNA, but **IET!** is ideal to treat small molecules like O_2.

The different branches produce almost the same result with the same **DCF!**; while `naive_interpolation` seems to be a bit more stable compared to `convolution` methods in terms of convergence, but have an energy shift about 2 kJ/mol.

The order of quadrature $m_{\max}$ has no influence to the energy and structure if it is larger than $n_{\max}$, while from $n_{\max} = 3$ the results begin to converge.

The spatial grid and angular grid have both an influence to the final results.

The defeat of **MDFT!** is that for very polar solutes, the grid needed should be very fine, and in 3D it is a very huge number, as it treats the same resolution from near to far from the solute.

$m\backslash n$	0	1	2	3	4	5
0	**0.00 (0.00)**	9.00 (3.00)	34.00 (18.00)	83.00 (39.00)	164.00 (84.00)	285.00 (139.00)
1	**0.00 (0.00)**	**0.00 (0.00)**	0.00 (1.67)	4.34 (6.07)	7.06 (13.63)	14.88 (17.30)
2	**0.00 (0.00)**	**0.00 (0.00)**	**0.00 (0.00)**	0.00 (0.00)	0.00 (0.00)	5.65 (2.71)
3	**0.00 (0.00)**	**0.00 (0.00)**	**0.00 (0.00)**	**0.00 (0.00)**	0.00 (0.00)	0.00 (0.00)
4	**0.00 (0.00)**	**0.00 (0.00)**	**0.00 (0.00)**	**0.00 (0.00)**	**0.00 (0.00)**	0.00 (0.00)
5	**0.00 (0.00)**	**0.00 (0.00)**	**0.00 (0.00)**	**0.00 (0.00)**	**0.00 (0.00)**	**0.00 (0.00)**

(a) $f(\mathbf{\Omega}) = 1$

$m\backslash n$	0	1	2	3	4	5
0	0.00 (0.00)	0.00 (0.00)	0.00 (0.00)	0.00 (0.00)	0.00 (0.00)	0.00 (0.00)
1	0.96 (0.96)	0.00 (0.00)	0.00 (0.00)	2.56 (6.99)	10.76 (14.15)	13.83 (21.21)
2	0.46 (0.46)	0.00 (0.00)	0.00 (0.00)	0.00 (0.00)	0.00 (0.00)	1.36 (0.50)
3	0.86 (0.86)	0.66 (0.66)	0.66 (0.66)	**0.00 (0.00)**	0.00 (0.00)	0.66 (0.66)
4	0.99 (0.99)	0.80 (0.80)	0.80 (0.80)	**0.00 (0.00)**	**0.00 (0.00)**	0.00 (0.00)
5	0.83 (0.83)	1.01 (1.01)	1.01 (1.01)	**0.00 (0.00)**	**0.00 (0.00)**	**0.00 (0.00)**

(b) $f(\mathbf{\Omega}) = \cos 3\Theta$

$m\backslash n$	0	1	2	3	4	5
0	0.00 (0.00)	9.00 (3.00)	34.00 (18.00)	83.00 (39.00)	164.00 (84.00)	285.00 (139.00)
1	0.00 (0.00)	0.00 (0.00)	0.00 (1.67)	4.34 (6.07)	7.06 (13.63)	14.88 (17.30)
2	1.00 (1.00)	1.00 (1.00)	0.50 (0.50)	1.53 (1.53)	1.15 (1.15)	3.65 (0.89)
3	1.00 (1.00)	1.00 (1.00)	1.00 (1.00)	0.83 (0.83)	1.10 (1.10)	1.11 (1.11)
4	1.00 (1.00)	1.00 (1.00)	1.00 (1.00)	0.90 (0.90)	0.90 (0.90)	0.69 (0.69)
5	1.00 (1.00)	1.00 (1.00)	1.00 (1.00)	0.94 (0.94)	0.94 (0.94)	0.80 (0.80)

(c) $f(\mathbf{\Omega}) = \cos 3\Phi$

$m\backslash n$	0	1	2	3	4	5
0	0.00 (0.00)	5.03 (1.68)	19.01 (10.06)	46.40 (21.80)	91.68 (46.96)	- (77.70)
1	0.00 (0.00)	0.00 (0.00)	0.00 (0.51)	1.32 (1.85)	2.15 (4.15)	4.53 (5.26)
2	0.56 (0.56)	0.56 (0.56)	0.07 (0.07)	0.55 (0.55)	0.76 (0.76)	2.05 (1.00)
3	0.47 (0.47)	0.47 (0.47)	0.47 (0.47)	**0.00 (0.00)**	0.46 (0.46)	0.46 (0.46)
4	0.56 (0.56)	0.56 (0.56)	0.56 (0.56)	**0.00 (0.00)**	**0.00 (0.00)**	0.00 (0.00)
5	0.51 (0.51)	0.51 (0.51)	0.51 (0.51)	**0.00 (0.00)**	**0.00 (0.00)**	**0.00 (0.00)**

(d) $f(\mathbf{\Omega}) = R^3_{30}(\mathbf{\Omega})$

Table 1.1: Maximum absolute error $E_a^{\max}$ of some function $f(\mathbf{\Omega})$ introduced by a forward-backward **GSHT!** process, with $s = 1$ outside the parentheses and $s = 2$ inside the parentheses; s being the **MRSO!** defined in §**??** concerning the C_{2v} symmetry. Differences that should be theoretically null (at machine precision) are shown in bold character and double underlined.

SOLUTE	$\mathfrak{q}$	σ [Å]	ϵ [kJ · mol^{-1}]
CH_4	-1.0 to 1.0	3.73	1.23

Table 1.4: Parameters of charged CH_4 LJ centers for test usage

METHOD	SURNAME	L	nfft/L	$m_{\max}$	$n_{\max}$
`naive_nmax1`	nmax1_lmn	24 to 60	3	1 (Leb), 3 angles for Ψ	1
`naive_interpolation`	nmax5_inter	24 to 60	3	2 (Leb), 3 angles for Ψ	5
`convolution_standard`	nmax1_convo	24 to 60	3	1	1

Table 1.5: Methods and parameters for charged CH_4 series test. Leb is Lebedev quadrature (6 angles of Θ and Φ for $m_{\max} = 1$ and 14 for $m_{\max} = 2$), which is mathematically equivalent with Gauss-Legendre quadrature but only ~2/3 angles.

CHARGE		-0.6			0			1	
$n_{\max}\backslash m_{\max}$	**IET!**	$= n_{\max}$	$= 5$	**IET!**	$= n_{\max}$	$= 5$	**IET!**	$= n_{\max}$	$= 5$
1	-157.48	diverge	-163.35	27.33	27.47	27.97	-382.34	-365.89	-379.01
2	-84.32	-87.56	-87.71	27.82	27.94	28.12	-301.74	-298.95	-298.67
3	-66.25	-69.58	-69.70	27.16	27.24	27.50	-294.77	-292.12	-291.87
4	no data	-69.41	-69.50	no data	27.85	27.91	no data	-289.19	-289.04
5	-66.50	diverge	diverge	27.25	27.47	27.47	-291.60	-288.54	-288.54

Table 1.6: Free energy of CH_4^q series (with corrections) for **IET!**, $m_{\max} = n_{\max}$ and $m_{\max} = 5$, using `convolution_standard`, with $L = 24$ Å, nfft = 72.

SOLUTE	SITE	q	σ [Å]	ϵ [kJ · mol^{-1}]	x [Å]
CO_2 [**Harris_1995**]	1	0.6512	2.76	0.234	0.000
(20.48 [kJ · mol^{-1}])	2	-0.3256	3.03	0.67	-1.149
	3	-0.3256	3.03	0.67	1.149
O_2 [**Boutard200525**]	1	0.0	3.1062	0.36	-0.485
(22.05 [kJ · mol^{-1}])	2	0.0	3.1062	0.36	0.485
	3	-2.1	0.00	0.00	-0.200
	4	-2.1	0.00	0.00	0.200
	5	4.2	0.00	0.00	0.000
N_2 [ref]	1	-0.5075	3.30	0.30	-0.549
(26.75 [kJ · mol^{-1}])	2	-0.5075	3.30	0.30	0.549
	3	1.0150	0.00	0.00	0.000

Table 1.8: Parameters of test solutes. Reference free energy by **IET!** in parentheses.

SOLUTE	CO_2 (20.48)		O_2 (22.05)		N_2 (26.75)	
$n_{\max}\backslash m_{\max}$	$m_{\max} = n_{\max}$	$m_{\max} = 5$	$m_{\max} = n_{\max}$	$m_{\max} = 5$	$m_{\max} = n_{\max}$	$m_{\max} = 5$
1	11.53	9.61	21.55	21.46	25.11	24.76
2	17.87	17.87	22.35	22.38	26.63	26.63
3	20.33	20.35	21.89	21.96	26.60	26.62
4	20.88	20.88	22.42	22.45	27.10	27.11
5	20.52	20.52	22.07	22.07	26.74	26.74

Table 1.9: Free energy of solutes. Reference free energy by **IET!** in parentheses.